IEEE Photonics Journal
An IEEE Photonics Society Publication

Open Access

Analysis of a Silicon Dual-Coupled-Ring Resonator Modulator Based on Push–Pull Coupling Tunings

Volume 10, Number 1, February 2018

Zhen Zhou
Li Shuang Feng

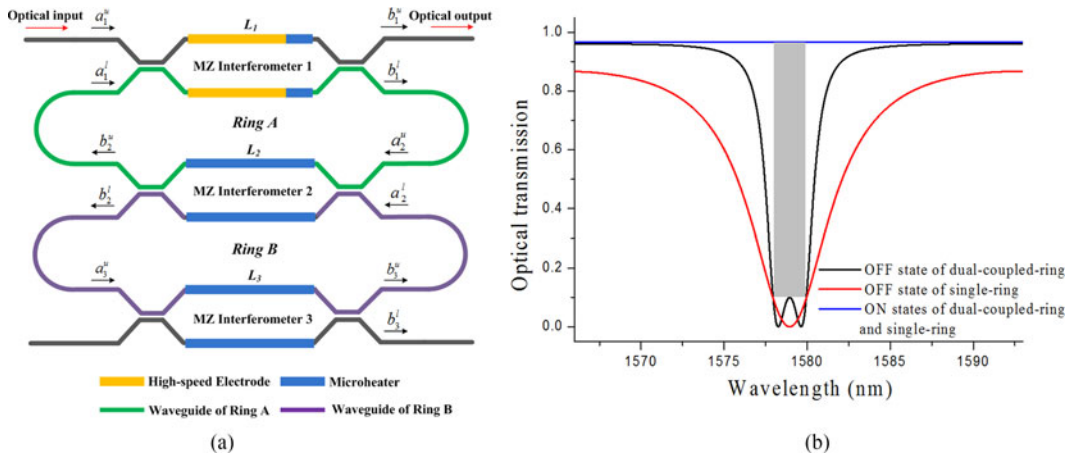

DOI: 10.1109/JPHOT.2017.2781689
1943-0655 © 2017 CCBY

Analysis of a Silicon Dual-Coupled-Ring Resonator Modulator Based on Push–Pull Coupling Tunings

Zhen Zhou and Li Shuang Feng

Key Laboratory on Inertial Science and Technology, School of Instrumentation Science and Opto-Electronics Engineering, Beihang University, Beijing 100191, China

DOI:10.1109/JPHOT.2017.2781689
This work is licensed under a Creative Commons Attribution 3.0 License. For more information, see http://creativecommons.org/licenses/by/3.0/

Manuscript received November 1, 2017; revised December 2, 2017; accepted December 5, 2017. Date of publication December 11, 2017; date of current version January 3, 2018. Corresponding author: Zhen Zhou (e-mail: zhouzhen@buaa.edu.cn).

Abstract: We present a silicon dual-coupled-ring resonator modulator with push–pull coupling tunings. The basic idea of this scheme is to construct a dual-coupled-ring resonator structure in which the coupling coefficients of all coupling regions are tunable through Mach–Zehnder interferometers operated in push–pull modes. Two coupling coefficients are tuned jointly for optical bandwidth shaping and tuning while another coupling coefficient is tuned for high speed and chirp-free modulation. The fundamental analytical expressions for the intensity transmittance, the critical and the resonance conditions of the proposed dual-coupled-ring resonator modulator are derived. In addition, the performance simulations and optimization are presented and compared with those of the single-ring resonator modulator. The proposed dual-coupled-ring resonator modulator is more likely to achieve wide optical bandwidth tuning range and narrow channel spacing simultaneously, which are suitable for future optical processing and interconnects.

Index Terms: Silicon, coupling tuning, dual-coupled-ring resonator, modulator, optical bandwidth, channel spacing.

1. Introduction

Silicon-based photonics which offers the potential to integrate photonics and electronics together on a single platform has generated an increasing interest in recent years, mainly for optical telecommunications or for optical interconnects. Silicon optical modulator is one of the critical CMOS-compatible integrated optoelectronic components to enable this breakthrough technology. High modulation speeds, low losses, large and tunable bandwidths and small footprints are crucial requirements for future on-chip optical processing and interconnects [1], [2].

Mach-Zehnder (MZ) interferometer [3], [4] and ring resonator [5], [6] are mainly two geometries available for achieving optical modulation. Compared with MZ interferometer, ring resonator has more potential for compact size and high density integration owing to its resonant nature. In principle, for a single ring resonator, three physical parameters including the index of the ring, the coupling between the ring and the bus waveguide and the loss of the ring can be varied to achieve the modulation. Compared with the modulations of index and loss, the coupling modulation can break the natural limitations on some characteristics such as the modulation bandwidth, chirp and so on [7]–[9]. Whatever modulation scheme is used, a high quality factor (Q) is desirable for a ring-resonator-based modulator to achieve low power consumption and high extinction ratio.

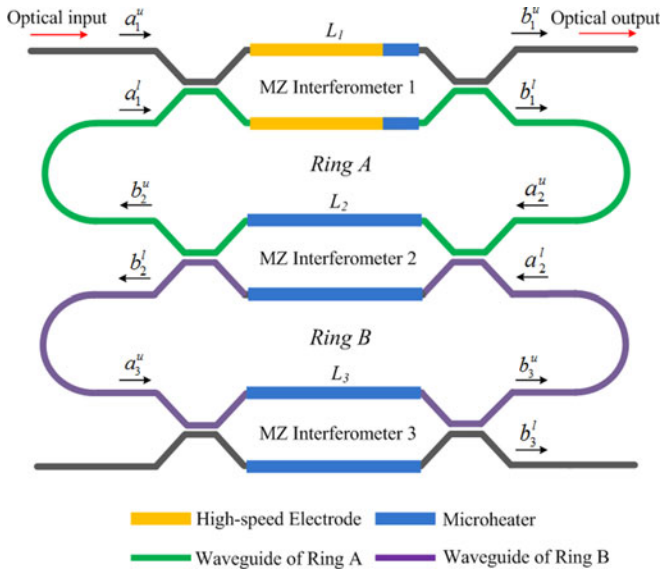

Fig. 1. Schematic diagram of the proposed dual-coupled-ring resonator modulator.

However, the relative narrow and spiky spectral features of a high-Q ring resonator make it sensitive to temperature variations and typical fabrication tolerances. The optical bandwidth and its thermal stability of a ring resonator can be improved by cascading multiple rings in either series-coupled-resonator [10], [11] or parallel-coupled-resonator [12], [13] configuration, both of which have been utilized in constructing silicon multiring resonator modulator schemes [14]–[24]. However, there are no reported modulator schemes applying the coupling modulation to the multiring resonator configuration, thus leading to the chirp and the bandwidth limitation imposed by the resonator linewidth. Moreover, the expanded optical bandwidths achieved in the reported schemes are not tunable, which greatly hamper their practical applications on optical process and interconnects. Meanwhile, the reported optical bandwidth-tunable ring resonator schemes [25], [26] are not used for modulating and are temperature-sensitive. Therefore, it would be meaningful to construct an innovative modulator which can combine the benefits of coupled-multiring resonator configuration and coupling modulation method to achieve better thermal stability, wider and tunable optical bandwidth, high modulation speed beyond linewidth limit and chirp-free modulation simultaneously, which are more applicable for future on-chip optical processing and interconnects. Motivated by this purpose, we propose a silicon dual-coupled-ring resonator modulator structure which has three coupling regions replaced by the MZ interferometers. Two MZ interferometers are tuned jointly for spectrum profile tailoring and another MZ interferometer is used to carry out the coupling modulation. In addition to the function of high-speed and chirp-free modulation with high thermal stability, the proposed dual-coupled-ring resonator modulator integrates a function of optical bandwidth tuning, which are suitable for optical signal processing such as reconfigurable filtering and routing in which the optical bandwidth can be tuned to accommodate one or more channels within one resonance. A theoretical analysis is provided to suggest the technical feasibility of the proposed scheme. The modulation performance simulations for the dual-coupled-ring resonator and the single-ring resonator configurations are presented and the corresponding results are compared.

2. Device Structure and Theory

Fig. 1 shows the schematic diagram of the proposed dual-coupled-ring resonator modulator. The silicon PIN waveguide configuration whose index can be manipulated by using the plasma dispersion effect [27] or the thermo-optic effect [28] is employed. For simplicity, the ring resonator

coupled to the through waveguide and the other ring resonator coupled to the drop waveguide are denoted as rings A and B, respectively. From the through waveguide to the drop waveguide, three MZ interferometers which are located in the three coupling areas are denoted by the numbers of 1, 2 and 3 respectively. For the MZ interferometer 1, its arms are equipped with a pair of high-speed electrodes for modulation and a pair of microheaters for bias-setting, respectively. For the two MZ interferometers 2 and 3, each of them is equipped with a pair of microheaters on its arms so that the two couplings can be controlled statically to achieve the desirable spectrum profile. In the following, a theory of dual-coupled-ring resonator modulator is established and the performance simulations for the proposed modulator structure are presented. Compared with the single-ring resonator scheme, the dual-coupled-ring resonator scheme combining the benefits of coupled-ring resonator configuration and coupling modulation way provides more latitude for optimization though the modeling gets more complicated.

Here, we consider the case in which the light is coupled to the upper waveguide of the MZ interferometer 1 and the through port of the ring A is taken as the output of the modulator, as shown in Fig. 1. In the formula derivation, we assume each MZ interferometer is operated in the push-pull mode so that a differential phase can be introduced between the two arms when a pair of opposite-sign driving voltages are applied on them. Meanwhile, we assume the propagation loss change caused by the applied voltage is ignored. Using the coupled mode theory, we can describe the input-output relations of the nth ($n = 1, 2, 3$) MZ interferometer sandwiched between two 3-dB couplers by [29]

$$\begin{pmatrix} b_n^u \\ b_n^l \end{pmatrix} = \exp[-(\alpha/2 + j\beta)L_n] \begin{pmatrix} -j\sin\frac{\Delta\phi_n}{2} & -j\cos\frac{\Delta\phi_n}{2} \\ -j\cos\frac{\Delta\phi_n}{2} & j\sin\frac{\Delta\phi_n}{2} \end{pmatrix} \begin{pmatrix} a_n^u \\ a_n^l \end{pmatrix} \tag{1}$$

where $a_n^{u,l}$ and $b_n^{u,l}$ are respectively the electric fields amplitudes in input and output ports of the nth MZ interferometer (refer to the notations in Fig. 1) and the propagating waves inside upper and lower waveguides of MZ interferometer are denoted by superscripts u and l respectively. α and $\beta = 2\pi n/\lambda$ are respectively the loss coefficient and the propagation constant of the waveguide, n is refractive index and λ is the wavelength. L_n and $\Delta\phi_n$ are the arm length of MZ interferometer and the differential phase between the two arms, respectively. For the coupling region which is replaced by the MZ interferometer driven in a push-pull mode, the coefficients of cross-coupling and self-coupling are $\cos(\Delta\phi_2/2)$ and $\sin(\Delta\phi_2/2)$, respectively.

Firstly, we consider the electric field amplitude in the ring B after propagating along the MZ interferometer 3. From (1), we can deduce the expression for b_3^u

$$b_3^u = -j\sin\frac{\Delta\phi_3}{2}\exp[-(\alpha/2 + j\beta)L_3]\, a_3^u \tag{2}$$

When we denote the perimeter of ring B as L_B and make use of (2), the transmission around the ring B can be written as

$$a_2^l = -j\sin\frac{\Delta\phi_3}{2}\exp[-(\alpha/2 + j\beta)(L_B - L_2)]\, b_2^l \tag{3}$$

Similarly, from (1), we can deduce the expression for the electric field amplitude in the ring B after propagating along the MZ interferometer 2

$$b_2^l = \exp[-(\alpha/2 + j\beta)L_2]\left(-j\cos\frac{\Delta\phi_2}{2}a_2^u + j\sin\frac{\Delta\phi_2}{2}a_2^l\right) \tag{4}$$

Combining (3) and (4), we obtain

$$a_2^l = \frac{\exp[-(\alpha/2 + j\beta)L_B]\cos\frac{\Delta\phi_2}{2}\sin\frac{\Delta\phi_3}{2}}{\exp[-(\alpha/2 + j\beta)L_B]\sin\frac{\Delta\phi_2}{2}\sin\frac{\Delta\phi_3}{2} - 1}a_2^u \tag{5}$$

We substitute (5) into (1) and obtain the expression for the electric field amplitude at the output port of upper waveguide of MZ interferometer 2

$$b_2^u = \frac{\exp\left[-\left(\frac{\alpha}{2}+j\beta\right)L_2\right]\left\{-j\exp\left[-\left(\frac{\alpha}{2}+j\beta\right)L_B\right]\sin\frac{\Delta\phi_3}{2}+j\sin\frac{\Delta\phi_2}{2}\right\}}{\exp\left[-\left(\frac{\alpha}{2}+j\beta\right)L_B\right]\sin\frac{\Delta\phi_2}{2}\sin\frac{\Delta\phi_3}{2}-1}a_2^u \tag{6}$$

Actually, (6) is electric field amplitude expression at the through port of a single ring whose two coupling coefficients are controlled by two MZ interferometers operated in the push-pull modes. Thus, when we denote the perimeter of ring A as L_A and make use of (6), the transmission around the ring A can be written as

$$a_1^l = \frac{\exp\left[-\left(\frac{\alpha}{2}+j\beta\right)(L_A-L_1)\right]\left\{-j\exp\left[-\left(\frac{\alpha}{2}+j\beta\right)L_B\right]\sin\frac{\Delta\phi_3}{2}+j\sin\frac{\Delta\phi_2}{2}\right\}}{\exp\left[-\left(\frac{\alpha}{2}+j\beta\right)L_B\right]\sin\frac{\Delta\phi_2}{2}\frac{\Delta\phi_3}{2}-1}b_1^l \tag{7}$$

Similarly, from (1), we can deduce the expression for the electric field amplitude in the ring A after propagating along the MZ interferometer 1

$$b_1^l = \exp\left[-\left(\frac{\alpha}{2}+j\beta\right)L_1\right]\left(-j\cos\frac{\Delta\phi_1}{2}a_1^u+j\sin\frac{\Delta\phi_1}{2}a_1^l\right) \tag{8}$$

Combining (7) and (8), we obtain

$$a_1^l = \frac{\cos\frac{\Delta\phi_1}{2}\sin\frac{\Delta\phi_3}{2}\exp\left[-\left(\frac{\alpha}{2}+j\beta\right)(L_A+L_B)\right]-\cos\frac{\Delta\phi_1}{2}\sin\frac{\Delta\phi_2}{2}\exp\left[-\left(\frac{\alpha}{2}+j\beta\right)L_A\right]}{\sin\frac{\Delta\phi_1}{2}\sin\frac{\Delta\phi_3}{2}\exp\left[-\left(\frac{\alpha}{2}+j\beta\right)(L_A+L_B)\right]-\sin\frac{\Delta\phi_1}{2}\sin\frac{\Delta\phi_2}{2}\exp\left[-\left(\frac{\alpha}{2}+j\beta\right)L_A\right]-\sin\frac{\Delta\phi_2}{2}\sin\frac{\Delta\phi_3}{2}\exp\left[-\left(\frac{\alpha}{2}+j\beta\right)L_B\right]+1}a_1^u \tag{9}$$

Substituting (9) into (1), we obtain the expression for the electric field amplitude transmittance of the proposed dual-coupled-ring resonator modulator

$$\frac{b_1^u}{a_1^u} = e^{-\left(\frac{\alpha}{2}+j\beta\right)L_1}\frac{je^{-\left(\frac{\alpha}{2}+j\beta\right)L_A}\left(\sin\frac{\Delta\phi_3}{2}e^{-\left(\frac{\alpha}{2}+j\beta\right)L_B}-\sin\frac{\Delta\phi_2}{2}\right)+j\sin\frac{\Delta\phi_1}{2}\left(1-\sin\frac{\Delta\phi_2}{2}\sin\frac{\Delta\phi_3}{2}e^{-\left(\frac{\alpha}{2}+j\beta\right)L_B}\right)}{-\sin\frac{\Delta\phi_1}{2}e^{-\left(\frac{\alpha}{2}+j\beta\right)L_A}\left(\sin\frac{\Delta\phi_3}{2}e^{-\left(\frac{\alpha}{2}+j\beta\right)L_B}-\sin\frac{\Delta\phi_2}{2}\right)-\left(1-\sin\frac{\Delta\phi_2}{2}\sin\frac{\Delta\phi_3}{2}e^{-\left(\frac{\alpha}{2}+j\beta\right)L_B}\right)} \tag{10}$$

When we introduce new parameters α_1, α_A, α_B, θ_A and θ_B defined by

$$\begin{cases}\alpha_1 = e^{-\alpha L_1/2}, \alpha_A = e^{-\alpha L_A/2}, \alpha_B = e^{-\alpha L_B/2} \\ \theta_A = \beta L_A, \theta_B = \beta L_B\end{cases} \tag{11}$$

Then the intensity transmittance of the proposed dual-coupled-ring resonator modulator is obtained as

$$T = \left|\frac{b_1^u}{a_1^u}\right|^2 = \left|\alpha_1\frac{j\alpha_A\alpha_B\sin\frac{\Delta\phi_3}{2}e^{-j(\theta_A+\theta_B)}-j\alpha_A\sin\frac{\Delta\phi_2}{2}e^{-j\theta_A}-j\alpha_B\sin\frac{\Delta\phi_1}{2}\sin\frac{\Delta\phi_2}{2}\sin\frac{\Delta\phi_3}{2}e^{-j\theta_B}+j\sin\frac{\Delta\phi_1}{2}}{-\alpha_A\alpha_B\sin\frac{\Delta\phi_1}{2}\sin\frac{\Delta\phi_3}{2}e^{-j(\theta_A+\theta_B)}+\alpha_A\sin\frac{\Delta\phi_1}{2}\sin\frac{\Delta\phi_2}{2}e^{-j\theta_A}+\sin\frac{\Delta\phi_2}{2}\sin\frac{\Delta\phi_3}{2}\alpha_B e^{-j\theta_B}-1}\right|^2 \tag{12}$$

where α_1 is the loss along one arm of MZ interferometers 1. α_i and θ_i (i = A,B) are the internal losses and the propagation phase shifts per circulation of ring A and B, respectively.

In order to achieve a high extinction ratio, the ring-resonator-based modulator is initially in the critical coupling condition in which the output is zero at specific wavelength corresponding to the critical coupling point. For the dual-coupled-ring resonator, there will be 2 critical coupling points due to the splitting of the original resonance as a result of coupling between the two rings resonators. This is in contrast to a single ring resonator in critical coupling condition, where the output is zero only when the light is fixed at the resonance, therefore resulting in a much narrower optical bandwidth. From (12), we can deduce the critical coupling condition for the proposed

dual-coupled-ring resonator modulator as

$$\sin\left(\frac{\Delta\phi_1}{2}\right) = \alpha_A \alpha_B \sin\left(\frac{\Delta\phi_3}{2}\right), (\Delta\phi_3 \neq 0) \tag{13}$$

where $\sin(\Delta\phi_3/2)$ is the self-coupling coefficient of the coupling region where the MZ interferometer 3 is located, namely the external loss of the ring B. The result indicates that the proposed dual-coupled-ring resonator is in the critical condition when the self-coupling coefficient of the coupling region where the MZ interferometer 1 is located equals the product of internal and external losses of the two coupled rings, similar to the critical condition in the single ring case [30]. When we assume the two rings have the same perimeter (i.e., $\alpha_A = \alpha_B$) and are in the critical coupling condition, the corresponding two critical coupling points are given by the following

$$\cos(\theta_{A,B}) = \frac{\alpha_B^2 \sin^2\left(\frac{\Delta\phi_3}{2}\right) + 1}{2\alpha_B \sin\left(\frac{\Delta\phi_3}{2}\right)} \sin\left(\frac{\Delta\phi_2}{2}\right) \tag{14}$$

The double-resonance condition can be derived from (14) as follows

$$tg\left(\frac{\Delta\phi_2}{4}\right) < \alpha_B \sin\left(\frac{\Delta\phi_3}{2}\right) \tag{15}$$

When $tg(\Delta\phi_2/4) = \alpha_B \sin(\Delta\phi_3/2)$ and the device is in the critical coupling condition, the two critical coupling points degenerate into a single critical point corresponding to resonance wavelength of a single ring resonator. When $tg(\Delta\phi_2/4) > \alpha_B \sin(\Delta\phi_3/2)$, the single-resonance still exists, but the critical coupling point disappears though the device is still in the critical coupling condition, and then the resonance depth decreases with the increasing differential phase $\Delta\phi_2$.

3. Transmission Spectrum Characteristics and Principle of Operation

In our simulation, we set the parameters of the proposed dual-coupled-ring resonator modulator as follows: the perimeters of the coupled dual rings are both 36 μm, the refractive index and loss coefficient of the silicon waveguide are 2.5 and 1/cm [17], respectively, the arm lengths of the three MZ interferometers are all 10 μm. The quality factor Q of the two rings are calculated to be both $\sim 10^5$. The waveguide has a typical width of 0.5 μm, a height of 0.25 μm, and a 50 nm-thick slab for p- and n-type doping along the arms of the MZ interferometers. The doping profile of the waveguide with a doping concentration of 1×10^{19} cm^{-3} is similar to that of the p-i-n diode in silicon microring resonator modulator [5], [31]. The simulation results indicate that there is one guided transverse-electric (TE) mode and one guided transverse-magnetic (TM) mode in the waveguide, in which only the TE mode is used. Considering three MZ interferometers and two ring resonators are employed, the polarization mode dispersion (PMD) would be an issue for the proposed dual-coupled-ring resonator modulator. Hence, the PMD compensators have to be used when the proposed dual-coupled-ring resonator modulator is used in the long-haul high bit-rate transmission systems [32]. When we assume the differential phase $\Delta\phi_3$ is π (i.e., external loss of ring B is zero) and the dual-coupled-ring resonator is critical coupled, Fig. 2(a) illustrates some typical transmission spectra with differential phase $\Delta\phi_2$. The corresponding cross-coupling coefficients (i.e., $\cos(\Delta\phi_2/2)$) of black line, blue line and red line are 0.047, 0.082 and 0.125, respectively. It is shown that two "split" critical coupling points caused by the coupling between the two coupled rings appear in the transmission spectrum with a peak in the center of them if the two coupled rings are set to have the same resonance wavelength. The two critical coupling points determined by (14) shift in opposite directions when $\Delta\phi_2$ varies, accompanied by the modifications of the width and height of the central peak which can be used for purpose of optical bandwidth tuning. The weaker the interaction between the coupled rings, the smaller the spacing between the two critical coupling points, and hence the lower and narrower the central peak. When the interaction reduces further to minimum (i.e., $\cos(\Delta\phi_2/2) = 0$), the two critical coupling points coincide and the central peak disappears. On the contrary, if the interaction is increased to maximum (i.e., $\cos(\Delta\phi_2/2) = 1$),

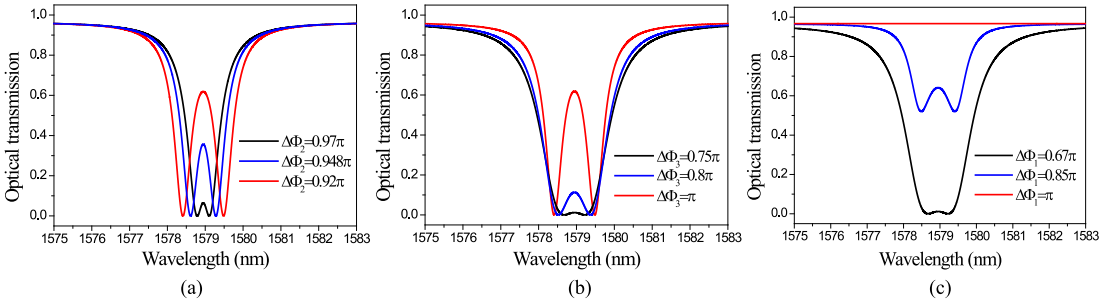

Fig. 2. Transmission spectrum of the dual-coupled-ring resonator (a) in the critical conditions with $\Delta\phi_2$ of 0.97π, 0.948π and 0.92π when $\Delta\phi_3$ is fixed, (b) in the critical condition with $\Delta\phi_3$ of 0.8π, 0.75π and π when $\Delta\phi_2$ is fixed, and (c) with $\Delta\phi_1$ of 0.67π, 0.85π *and* π when $\Delta\phi_2$ and $\Delta\phi_3$ are fixed.

the spacing between the two critical coupling points and the height of the central peak reach the maximums simultaneously. Therefore, the stronger cross-coupling between the coupled two rings resonators helps achieve the wider optical bandwidth.

Besides a wide bandwidth, a flat optical bandwidth is beneficial for the insensitivity to fabrication and temperature variations. However, it can be seen in Fig. 2(a) that the optical bandwidth width extends at the expense of its flatness for the case in which the differential phase $\Delta\phi_3$ is fixed. This tradeoff can be alleviated by controlling the coupling between drop waveguide and ring B to produce external loss for ring B. When other parameters are kept unchanged and $\Delta\phi_2 = 0.92\pi$ is given, Fig. 2(b) illustrates some typical transmission spectra with differential phase $\Delta\phi_3$ when the dual-coupled-ring resonator is critical coupled. The corresponding external losses of ring B (i.e., cross-coupling coefficient $\cos(\Delta\phi_3/2)$ of black line, blue line and red line are 0.383, 0.309 and 0, respectively. One can observe from Fig. 2(b) that, for a given $\Delta\phi_2$, the central peak between the two critical coupling points gets lower and the stopband gets more flat accordingly with the increasing external loss of ring B whereas the spacing between the two critical points reduces slightly. Thus, by tuning the two coupling coefficients of coupling regions where the MZ-interferometers 2 and 3 are located jointly, it may be possible to get the tunable spectrum shape with the desired width and flatness of the optical bandwidth.

The MZ interferometer 1 is initially biased by a pair of microheaters using the thermo-optic effect so that the proposed dual-coupled-ring resonator modulator is critical coupled (i.e., the critical coupling condition (13) is satisfied) and thereby is in the OFF state. The modulation operation is accomplished by applying a pair of opposite-sign driving voltages to the two arms of the MZ interferometer 1 through the high-speed electrodes using the plasma dispersion effect. Fig. 2(c) shows the spectra change with the cross-coupling coefficient $\cos(\Delta\phi_1/2)$ when the flattened optical bandwidth is fixed (i.e., the differential phases $\Delta\phi_2$ and $\Delta\phi_3$ are fixed). The corresponding cross-coupling coefficients $\cos(\Delta\phi_1/2)$ of black line, blue line and red line are 0.495, 0.233 and 0, respectively. We can observe that the resonance depth of the spectrum is modified when the push-pull coupling tuning is used in the MZ interferometer 1, whereas the resonance remains unshifted and the notch profile almost keeps unchanged, resulting in a chirp-free intensity modulation covering an expanded wavelength range. When the differential phase $\Delta\phi_1$ is tuned to be π (i.e., the self-coupling coefficient is 1), the proposed dual-coupled-ring resonator modulator is switched to the ON state in which there is no optical power transmitting through the ring A and the insertion loss is mainly determined by the propagation loss along one arm of the MZ interferometer 1. We can observe from Fig. 2(c) that a broad and flat spectrum response with a high transmission ($>$98%) can be achieved for the ON state, corresponding to an insertion loss of less than 0.1 dB. When the differential phase $\Delta\phi_1$ is tuned to be 0.67π (i.e., the dual-ring resonator is critical coupled), the OFF state has below 2% transmission for an expanded wavelength range, corresponding to an extinction ratio of $\sim$17 dB, which is advantageous to carry out the high-depth and wide-optical bandwidth modulation. The modulation depth is calculated to be $\sim$17 dB by $10\log(I_{max}/I_{min})$, where

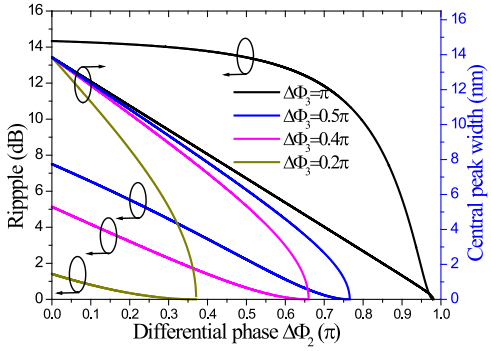

Fig. 3. The central peak width w_c and ripple r versus the differential phase $\Delta\phi_2$ for several differential phases $\Delta\phi_3$.

I_{max} and I_{min} are intensities transmitted when the modulator is switched to ON state and OFF state, respectively.

When the PIN diode structure of the proposed dual-coupled-ring resonator modulator is forward biased, the modulation bandwidth is mainly determined by the free carrier lifetime and the photon cavity lifetime. As the modulation of the proposed dual-coupled-ring resonator modulator is accomplished by coupling tuning so that the modulation bandwidth is only determined by the non-resonant MZ interferometer and the linewidth limitation on modulation bandwidth can be broken [7], [9]. Considering the effective carrier lifetime 100 ps can be achieved by using carrier lifetime reduction scheme [31], [33], the modulation bandwidth is estimated to be ~10 GHz.

4. Performance Simulation and Comparison

In this section, optical bandwidth, channel space and combined bandwidth-spacing performance of the proposed dual-coupled-ring resonator modulator are simulated and optimized, and the corresponding results are compared with those of the single-ring resonator modulator. The optical structure parameters of the modulator and the assumptions have been given above.

4.1 Optical Bandwidth

The goal of this analysis is to design a dual-coupled-ring resonator modulator with a wide and flat optical bandwidth. To facilitate the optical bandwidth analysis, the central peak width w_c, defined as the spacing between two critical points and the ripple r of the spectrum stopband are used to characterize the width and the flatness of the optical bandwidth, respectively. Fig. 3 shows the variations of central peak width w_c and ripple r with differential phases $\Delta\phi_2$ and $\Delta\phi_3$. It is shown in Fig. 3 that the central peak width w_c increases with the increasing coupling between the two ring resonators (i.e., the decreasing of differential phase $\Delta\phi_2$) for a fixed external loss of the ring B (i.e., the fixed differential phase $\Delta\phi_3$), which can be used for purpose of optical bandwidth expanding or tuning. However, as shown in Fig. 3, for the case in which there is no external loss in ring B (i.e., $\Delta\phi_3 = \pi$), the ripple becomes larger rapidly and then keeps a large value with the increasing central peak width, which limits optical bandwidth expanding greatly. As we have analyzed in the previous section, the combined flatness-width limitation can be alleviated by introducing the external loss in ring B. As shown in Fig. 3, for the cases involving external loss in ring B (i.e., $\Delta\phi_3 \neq \pi$), the ripple increases relatively slowly with the increasing central peak width and the lower ripple can be achieved for the higher external loss when the central peak width is fixed, which is beneficial to achieve wide and flat optical bandwidth simultaneously.

Optical bandwidth refers to the useful operational wavelength range of a device [1]. As the spectrum response for the ON state is broad and flat, the optical bandwidth of the dual-coupled-ring

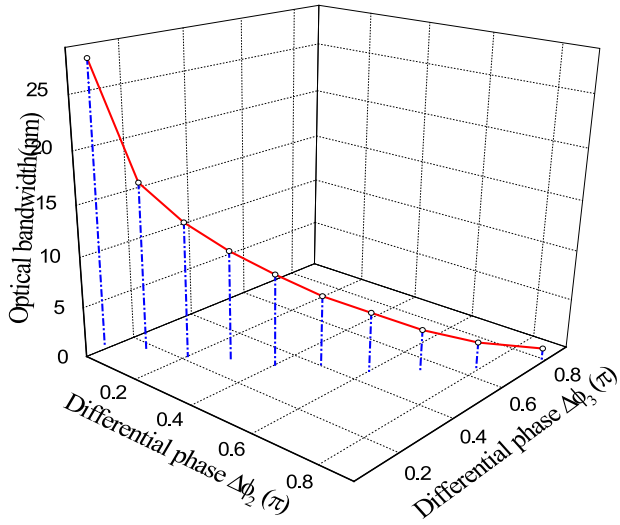

Fig. 4. The optimum combinations of the differential phases $\Delta\phi_2$ and $\Delta\phi_3$ and the resulting optical bandwidth.

resonator modulator is mainly determined by the spectrum shape in the OFF state. Therefore, in order to evaluate the combined width-flatness performance of the optical bandwidth, here we defined the optical bandwidth of the modulator to be the width of the continuous wavelength region where the transmission is below 10% in the OFF state, corresponding to an extinction ratio of ~10 dB. Obviously, according to the definition, the optical bandwidth reaches the maximum when the transmission of central peak between the two critical coupling points is 10%. Fig. 4 shows the optimum combinations of the differential phases $\Delta\phi_2$ and $\Delta\phi_3$ for the maximum optical bandwidth. We can observe from Fig. 4 that a wide tuning range of optical bandwidth (~28 nm) can be achieved by tuning the differential phases $\Delta\phi_2$ and $\Delta\phi_3$ jointly, and the optical bandwidth expanding requires the decreases of differential phases $\Delta\phi_2$ and $\Delta\phi_3$.

4.2 Channel Spacing

Although the wide optical bandwidth is beneficial to decrease the sensitivity to the temperature and fabrications variations, it results in the increase of channel spacing if the proposed dual-coupled-ring resonator modulators are cascaded to form a wavelength-division-multiplexing (WDM) modulation system. Meanwhile, similar to the single ring resonator, the increase of external loss which is utilized to alleviate the combined width-flatness limitation of the dual-coupled-ring resonator may decrease the sharpness of the rising and falling edges and the out-of-band pass ratio due to the Q degradation, thus inducing a significant insertion loss and inter-channel-interference modulation to the adjacent channel and subsequently a low spectral efficiency if the channel spacing is not large enough. For comparison, Fig. 5 shows the transmission spectra of single-ring resonator and dual-coupled-ring resonator modulators when both of the optical bandwidths reach 2 nm (gray region) which is enough to accommodate a temperature drift of ±15 °C without degrading device performance [34]. In this comparison, we assume both of the two ring-resonator-based modulators utilize the coupling modulation method and have the same ring resonator parameters. From Fig. 5 we can see that, compared with the single-ring resonator scheme, the proposed dual-coupled-ring resonator scheme has a higher and flatter pass band and a sharper resonance than the single ring due to the higher Q-factor. This means, with the same optical bandwidth and ring parameters, the single-ring resonator scheme introduces a larger insertion loss and inter-channel interference modulation than the dual-coupled-ring resonator scheme. For example, for the single ring resonator scheme, if an adjacent wavelength channel is placed 3 nm from the central wavelength of this

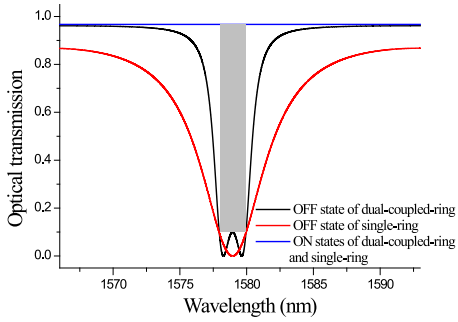

Fig. 5. The transmission spectra of single-ring resonator and dual-coupled-ring resonator modulators when both of the optical bandwidths reach 2 nm.

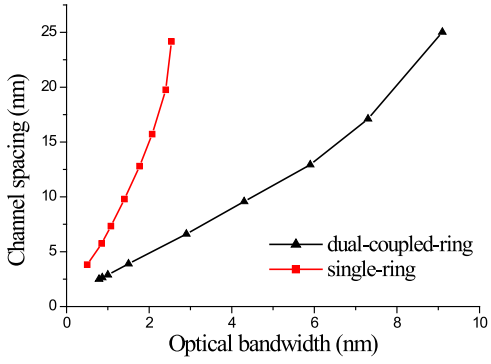

Fig. 6. Minimum channel spacing as functions of the optical bandwidth for the dual-coupled-ring resonator and the single-ring resonator modulators when 0.97 dB adjacent channel insertion loss is acceptable.

channel (1579 nm), a small insertion loss of 0.5 dB and a low inter-channel interference modulation of 0.35 dB are introduced for the dual-coupled-ring resonator modulator. However, for the same channel placement, the single-ring resonator modulator with the same optical bandwidth introduces a 3.25 dB insertion loss and a 3.1 dB inter-channel interference modulation thus results in much larger channel spacing. If we assume a 0.97 dB adjacent channel insertion loss which corresponds to 80% transmission of spectrum passband is acceptable to a WDM system, the minimum channel spacing is $S = 0.5\ BW_{0.97dB}$ where $BW_{0.97dB}$ is 0.97 dB optical bandwidth. Fig. 6 shows the minimum channel spacing as functions of the optical bandwidth for the dual-coupled-ring resonator modulator and the single-ring resonator modulator. As shown in Fig. 6, the curve slope of the proposed dual-coupled-ring resonator modulator is much smaller than that of the single-ring resonator modulator, which means it has a higher spectral capacity. For example, with the same optical bandwidth of 2 nm and ring resonator parameters, the necessary channel spacing of the dual-coupled-ring resonator modulator is 4.9 nm and 3 times smaller than that of the single-ring resonator modulator, which also corresponds 3 times higher spectral capacity.

4.3 Combined Bandwidth-Spacing

As analyzed in the previous section, there is a tradeoff between the optical bandwidth and the minimum channel spacing whether configuration is single-ring resonator or dual-coupled-ring resonator. Consequently, it is difficult to simultaneously optimize these parameters. In order to evaluate the combined bandwidth-spacing performance, we have defined a figure-of-merit (FOM) to be the ratio between the optical bandwidth defined above and $BW_{0.97dB}$, considering the minimum channel

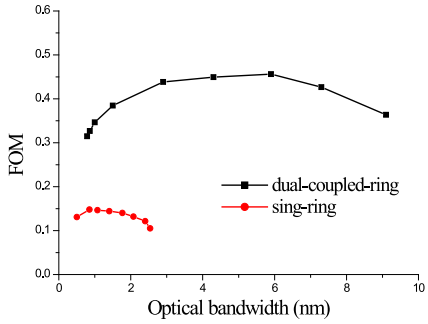

Fig. 7. FOMs as functions of optical bandwidth for the dual-coupled-ring resonator and the single-ring resonator cases.

spacing is proportional to the optical bandwidth determined by the acceptable adjacent channel insertion loss (0.97 dB is assumed in this paper). The wider the optical bandwidth and the smaller the channel spacing, the larger will be the FOM. Thus, the maximum FOM provides a good compromise between the optical bandwidth and the channel spacing. Fig. 7 shows the defined FOMs as functions of optical bandwidth for the dual-coupled-ring resonator and the single-ring resonator modulators. Obviously, the overall FOM curve of dual-coupled-ring resonator modulator is much higher than that of the single-ring resonator modulator which means it is more likely to achieve the wide optical bandwidth and the narrow channel spacing simultaneously. Moreover, it can be found in Fig. 7 that the dual-coupled-ring resonator modulator is superior to the single-ring resonator modulator in the optical bandwidth tuning range which means more channels can be accommodated when it is used as a reconfigurable channel selector for WDM system.

5. Power Consumption Estimation and Analysis

The power consumption defined as the energy expended in producing each bit of data is an important parameter to characterize the modulator used for optical interconnects [1]. Although high thermal stability, tunability of optical bandwidth, chirp-free modulation and high speed modulation beyond linewidth limitation can be achieved for the proposed dual-ring resonator modulator, the integration of ring resonators and MZ interferometers may result in the higher power consumption. In this section, we estimate and analyze the power consumption of the proposed dual-coupled-ring resonator modulator.

To facilitate the estimation of power consumption, we make the assumption that the structures of p-i-n diode employed in the proposed device are the same with that in the reference [31], so we use the optimum driving results in this reference and set the bias voltage and drive voltage to be 1.13 V and 540 mV respectively. The total energy consumption for modulation comprises of dynamic and DC parts. The dynamic energy consumption defined as the total charge injected to the p-i-n diode times voltage swing can be evaluated by the following equation [31]

$$Energy/bit = 1/8 \times e \times (\Delta N_e + \Delta N_h) \times Vol \times V_{pp} \tag{16}$$

where $e = 1.602 \times 10^{-19}$ C is the electron charge, $Vol = S \times L$ is the modal volume of the waveguide section with an effective modal area of S = 0.25 μm $\times$ 0.5 μm = 0.125 μm^2, L is the arm length of MZ interferometer, V_{pp} is the peak-to-peak drive voltage, and $\triangle N_e$ and $\triangle N_h$ are the densities of injected electron and hole which are 5.5 $\times$ 10^{17} when a drive voltage of V_{pp} = 540 mV is applied. The estimated result of dynamic energy consumption is ~29 fJ/bit. The DC power consumption of the proposed device is approximately given by $P_{DC} = V_{ON} I_{ON}$, where the bias voltage $V_{ON} = 1.13$ V and the corresponding current through the PIN diode $I_{ON} = e \times \rho \times Vol/\tau_c = \sim 0.56$ mA with the effective carrier lifetime $\tau_c \asymp 100$ ps allowing for a modulation bandwidth of 10 GHz, the steady state carrier density $\rho = 2.8 \times 10^{17}$ cm^{-3} under the bias voltage of 1.13 V. When the modulation

speed is 10 GHz, the DC energy consumption is estimated to be ∼63.3 fJ/bit. Thus, the total energy consumption for modulation is ∼92.3 fJ/bit which is dominated by the DC energy consumption.

In addition to the power consumption for modulation, the extra power consumed by the micro-heaters for optical bandwidth shaping and tuning is required for the proposed dual-coupled-ring resonator modulator. It has been experimentally demonstrated that a 500 μm silicon waveguide length can deliver a phase shift of π for an applied power of 10 mW [35], thus the power consumption for a MZ interferometer whose arm length of thermo tuning is 10 μm operated in a push-pull mode would be ∼250 mW. Considering there are three MZ interferometers in the proposed dual-ring resonator modulator, the maximum power consumption caused by the heaters would be ∼750 mW. Through the estimation of power consumption, we observe the power consumption of optical bandwidth shaping and tuning dominates the total energy of the proposed dual-ring resonator modulator.

6. Conclusion

In this paper, a silicon dual-coupled-ring resonator modulator whose coupling regions are replaced by three MZ interferometers has been proposed and analyzed theoretically. The transmission spectrum characteristics at different coupling coefficients of three coupling regions have been analyzed and optimized. It was shown that a wide, flat and tunable spectrum response can be easily achieved by tuning the two MZ interferometers while a high-speed and chirp-free intensity modulation is carried out by tuning the another MZ interferometer for the proposed dual-coupled-ring resonator modulator. The performances of the dual-coupled-ring resonator modulator are simulated and optimized. Compared with the single-ring resonator modulator, the dual-coupled-ring resonator modulator has three advantages, i.e., wider optical bandwidth, better thermal stability, and most importantly, the tunability of optical bandwidth and chirp-free modulation. Hence, it shows better combined bandwidth-space and bandwidth tuning properties and is more applicable for future on-chip optical processing and interconnects. However, the dual-coupled-ring resonator and microheaters introduce the disadvantages of a larger footprint and power consumption, which can be reduced by optimizing the structures and geometries of the waveguide [25] and microheater [31], [36].

References

[1] G. T. Reed, G. Mashanovich, F. Y. Gardes, and D. J. Thomson, "Silicon optical modulators," *Nature Photon.*, vol. 4, no. 8, pp. 518–526, Aug. 2010.
[2] B. G. Lee, A. Biberman, J. Chan, and K. Bergman, "High-performance modulators and switches for silicon photonic networks-on-chip," *IEEE J. Sel. Topics Quantum Electron.*, vol. 16, no. 1, pp. 6–22, Jan./Feb. 2010.
[3] J. W. Park, J. B. You, I. G. Kim, and G. Kim, "High-modulation efficiency silicon Mach-Zehnder optical modulator based on carrier depletion in a PN diode," *Opt. Exp.*, vol. 17, no. 18, pp. 15520–15524, Aug. 2009.
[4] P. Dong, L. Chen, and Y. Chen, "High-speed low-voltage single-drive push-pull silicon Mach-Zehnder modulators," *Opt. Exp.*, vol. 20, no. 6, pp. 6163–6169, Mar. 2012.
[5] Q. Xu, B. Schmidt, S. Pradhan, and M. Lipson, "Micrometre-scale silicon electro-optic modulator," *Nature*, vol. 435, no. 7040, pp. 325–327, May 2005.
[6] P. Dong *et al.*, "Low Vpp, ultralow-energy, compact, high-speed silicon electro-optic modulator," *Opt. Exp.*, vol. 17, no. 25, pp. 22484–22490, Dec. 2009.
[7] W. D. Sacher and J. K. S. Poon, "Dynamics of microring resonator modulators," *Opt. Exp.*, vol. 16, no. 20, pp. 15741–15753, Sep. 2008.
[8] T. Ye, Y. Zhou, C. Yan, Y. Li, and Y. Su, "Chirp-free optical modulation using a silicon push-pull coupling microring," *Opt. Lett.*, vol. 34, no. 6, pp. 785–787, Mar. 2009.
[9] W. D. Sacher *et al.*, "Coupling modulation of microrings at rates beyond the linewidth limit," *Opt. Exp.*, vol. 21, no. 8, pp. 9722–9733, Apr. 2013.
[10] A. Melloni, "Synthesis of a parallel-coupled ring-resonator filter," *Opt. Lett.*, vol. 26, no. 12, pp. 917–919, Jun. 2001.
[11] Q. Xu, P. Dong, and M. Lipson, "Breaking the delay-bandwidth limit in a photonic structure," *Nature Phys.*, vol. 3, pp. 406–410, Apr. 2007.
[12] S. Xiao, M. H. Khan, H. Shen, and M. Qi, "A highly compact third-order silicon microring add-drop filter with a very large free spectral range, a flat passband and a low delay dispersion," *Opt. Exp.*, vol. 15, no. 22, pp. 14765–14771, Oct. 2007.
[13] F. Xia, M. Rooks, L. Sekaric, and Y. Vlasov, "Ultra-compact high order ring resonator filters using submicron silicon photonic wires for on-chip optical interconnects," *Opt. Exp.*, vol. 15, no. 19, pp. 11934–11941, Sep. 2007.

[14] Q. Xu, B. Schmidt, J. Shakya, and M. Lipson, "Cascaded silicon micro-ring modulators for WDM optical interconnection," *Opt. Exp.*, vol. 14, no. 20, pp. 9430–9435, Oct. 2006.
[15] Q. Xu, "Silicon dual-ring modulator," *Opt. Exp.*, vol. 17, no. 23, pp. 20783–20793, Nov. 2009.
[16] Y. Li *et al.*, "Coupled-ring-resonator-based silicon modulator for enhanced performance," *Opt. Exp.*, vol. 16, no. 17, pp. 13342–13348, Aug. 2008.
[17] T. Ye and X. Cai, "On power consumption of silicon-microring-based optical modulators," *J. Lightw. Technol.*, vol. 28, no. 11, pp. 1615–1623, Jun. 2010.
[18] R. A. Integlia, L. Yin, D. Ding, D. Z. Pan, D. M. Gill, and W. Jiang, "Parallel-coupled dual racetrack micro-resonators for quadrature amplitude modulation," *Opt. Exp.*, vol. 19, no. 16, pp. 14892–14902, Jul. 2011.
[19] S. Akiyama and S. Nomura, "Dynamic response of modulators based on cascaded-ring-resonator," *Opt. Exp.*, vol. 20, no. 20, pp. 21847–21859, Sep. 2012.
[20] T. Gu, Y. Chen, C. W. Wong, and P. Dong, "Cascaded uncoupled dual-ring modulator," *Opt. Lett.*, vol. 39, no. 16, pp. 4974–4977, Aug. 2014.
[21] H. Yu *et al.*, "Silicon dual-ring modulator driven by differential signal," *Opt. Lett.*, vol. 39, no. 22, pp. 6379–6382, Nov. 2014.
[22] A. Hosseinzadeh and C. T. Middlebrook, "Highly linear dual ring resonator modulator for wide bandwidth microwave photonic links," *Opt. Exp.*, vol. 24, no. 24, pp. 27268–27279, Nov. 2016.
[23] B. Haq and M. Rasras, "Broadband and high-speed silicon dual-ring modulator based on p-i-n-i-p junction," *Proc. SPIE*, vol. 9891, pp. 9891101–9891107, 2016.
[24] X. Sun, L. Zhou, M. Jager, D. Petousi, L. Zimmermann, and K. Petermann, "Silicon dual-ring resonator-based push-pull modulators," *Proc. SPIE*, vol. 9752, pp. 97520801–97520806, 2016.
[25] L. Chen, N. S. Droz, and M. Lipson, "Compact bandwidth-tunable microring resonators," *Opt. Lett.*, vol. 32, no. 22, pp. 3361–3363, Nov. 2007.
[26] E. Pawlowski *et al.*, "Variable bandwidth and tunable centre frequency filter using transversal-form programmable optical filter," *Electron. Lett.*, vol. 32, no. 2, pp. 113–114, Jan. 1996.
[27] G. T. Reed and A. P. Knights, "Optical modulation mechanisms in silicon," in *Silicon Photonics: An introduction*. Chichester, U.K.: Wiley, 2004, pp. 97–103.
[28] G. Cocorullo and I. Rendina, "Thermal-optical modulation at 1.5 μm in silicon etalon," *Electron. Lett.*, vol. 28, no. 1, pp. 83–85, 1992.
[29] T. Ye, Y. Zhou, C. Yan, Y. Li, and Y. Su, "Chirp-free optical modulation using a silicon push-pull coupling microring," *Opt. Lett.*, vol. 34, no. 6, pp. 785–787, Mar. 2009.
[30] A. Yariv, "Universal relations for coupling of optical power between microresonators and dielectric waveguides," *Electron. Lett.*, vol. 36, no. 4, pp. 321–322, Feb. 2000.
[31] T. Wang, M. Xu, F. Li, J. Y. Wu, L. J. Zhou, and Y. K. Su, "Design of a high-modulation-depth, low-energy silicon modulator based on coupling tuning in a resonance-split microring," *J. Opt. Soc. Amer. B*, vol. 29, no. 11, pp. 3047–3056, Nov. 2012.
[32] Katsunari Okamoto, *Fundamentals of Optical Waveguides*. Amsterdam, The Netherlands: Elsevier, 2006, ch. 9, pp. 522–523.
[33] N. M. Wright *et al.*, "Free carrier lifetime modification in silicon," *Proc. SPIE*, vol. 7220, 2009, Art. no. 722006.
[34] Y. Vlasov, W. M. J. Green, and F. Xia, "High-throughput silicon nanophotonic wavelength-insensitive switch for on-chip optical networks," *Nature Photon.*, vol. 2, pp. 242–246, Apr. 2008.
[35] G. T. Reed and A. P. Knights, *Silicon Photonics: An Introduction*. New York, NY, USA: Wiley, 2004, ch. 4, pp. 97–103.
[36] S. Yan *et al.*, "Slow-light-enhanced energy efficiency for graphene microheaters on silicon photonic crystal waveguides," *Nature Commun.*, vol. 8, 2017, Art. no. 14411.